

Training Latent Diffusion Models with Interacting Particle Algorithms

Tim Y. J. Wang^{*1}, Juan Kuntz, and O. Deniz Akyildiz^{†1}

¹Department of Mathematics, Imperial College London

June 10, 2025

Abstract

We introduce a novel particle-based algorithm for end-to-end training of latent diffusion models. We reformulate the training task as minimizing a free energy functional and obtain a gradient flow that does so. By approximating the latter with a system of interacting particles, we obtain the algorithm, which we underpin theoretically by providing error guarantees. The novel algorithm compares favorably in experiments with previous particle-based methods and variational inference analogues.

1 Introduction

Diffusion Models (DMs) introduced in [Sohl-Dickstein et al. \(2015\)](#), and further developed in [Ho et al. \(2020\)](#); [Song et al. \(2021c\)](#), excel in numerous generative modelling tasks. Examples include image synthesis ([Dhariwal and Nichol, 2021](#)), protein design ([Watson et al., 2023](#)), and language modelling ([Nie et al., 2025](#)). They work by progressively adding noise to data to transform the data distribution into an easy-to-sample reference distribution, and then learn to revert this noising process. However, these steps take place in the data’s *ambient* space which is typically high dimensional. For this reason, DM training and inference proves computationally expensive. To alleviate this issue, [Rombach et al. \(2022\)](#); [Vahdat et al. \(2021\)](#); [Wehenkel and Louppe \(2021\)](#) and others proposed using a Variational Autoencoder (VAE) ([Kingma and Welling, 2013](#)) to map back-and-forth between the high-dimensional ambient space and a low-dimensional *latent* space, and carrying out the noising/de-noising steps in the latter. To date, the world’s most popular DMs (e.g., [Podell et al. \(2024\)](#)) fall into this Latent Diffusion Model (LDM) category.

Recently, [Kuntz et al. \(2023\)](#); [Lim et al. \(2024\)](#); [Lim and Johansen \(2024\)](#) have reported performance gains when training simpler latent-variable models and related tasks by replacing variational approximations with particle-based ones. Here, we investigate whether this is also the case for LDMs and introduce the, to the best of our knowledge, first particle-based method for LDM training.

Contributions.

- (C1) We recast the problem of LDM training as the minimization of a free energy functional, characterize the functional’s minima (Proposition 2.1), identify a gradient flow that minimizes it, and establish its exponential convergence under standard assumptions (Theorem 3.1).
- (C2) Approximating the flow in (C1), we obtain Interacting Particle Latent Diffusions (IPLDs)—a simple, particle-based, and encoder-free, algorithm for LDM training well-adapted to modern compute environments—and we derive non-asymptotic bounds on its error (Theorem 3.2).

^{*}Corresponding author. tw1320@ic.ac.uk

[†]deniz.akyildiz@imperial.ac.uk

- (C3) Through several practical improvements, we obtain an efficient and scalable version of the algorithm (Section 3.3) and demonstrate its effectiveness in numerical experiments (Section 5).
- (C4) Lastly, by approaching LDMs from the above unexplored angle, we open the door to other novel LDM training methods. In particular, our approach connects latent diffusion models to the rich body of work on gradient flows and interacting particle systems stemming from the optimal transport literature (Villani et al., 2008; Chaintron and Diez, 2022)—a connection that can spur the design of new algorithms as we demonstrate here.

Paper structure. The paper is organized as follows. First, we review the necessary background on LDMs and identify relevant loss functions (Section 2). Next, we obtain IPLD: an algorithm for minimizing this loss (Section 3). We do so by, identifying a gradient flow that minimizes the loss (Section 3.1), approximating it (Section 3.2), and incorporating a series of practical improvements (Section 3.3). We then survey the related literature (Section 4) and experimentally compare IPLD with relevant baselines (Section 5). We conclude with a discussion of our results, IPLD’s limitations, and future research directions (Section 6).

Notation. We use $\mathsf{X} = \mathbb{R}^{d_x}$ and $\mathsf{Z} = \mathbb{R}^{d_z}$ to denote the ambient and latent spaces, $\Theta = \mathbb{R}^{d_\theta}$ and $\Phi = \mathbb{R}^{d_\phi}$ the decoder’s and DM’s parameter spaces (c.f. Section 2), $\{x_1, \dots, x_M\}$ the training set, and $\mathcal{P}(\mathbb{R}^d)$ the space of probability distributions on \mathbb{R}^d .

2 Background on latent diffusion models

We consider latent-space versions of Denoising Diffusion Probabilistic Models (DDPMs) Ho et al. (2020) similar to those in Rombach et al. (2022); Vahdat et al. (2021); Wehenkel and Louppe (2021):

$$p_{\theta, \phi}(x, z_{0:K}) = p_\phi(x|z_0)p_\theta(z_{0:K}) \quad (1)$$

where $p_\phi(x|z_0) = \mathcal{N}(x; g_\phi(z_0), \sigma^2 I)$ is an isotropic Gaussian decoder, with $g_\phi : \mathsf{Z} \rightarrow \mathsf{X}$ denoting a neural network, parametrized by ϕ , that maps from the latent space to the ambient space, and the prior,

$$p_\theta(z_{0:K}) := p(z_K) \prod_{k=1}^K p_{\theta, k}(z_{k-1}|z_k),$$

is a DDPM parametrized by θ . The DDPM’s distribution at time K is a standard Gaussian, $p_K(z_K) := \mathcal{N}(z_K; 0, I)$, and the backward kernels are also Gaussian: $p_{\theta, k}(z_{k-1}|z_k) := \mathcal{N}(z_{k-1}; \mu_{\theta, k}(z_k), \beta_k^2 I)$ where $(k, z) \mapsto \mu_{\theta, k}(z)$ denotes a neural network, parametrized by θ , that maps from $\{1, \dots, K\} \times \mathsf{Z}$ to Z and $\{\beta_k\}_{k=1}^K$ a fixed noise schedule.

We fit the model by searching for parameters $(\theta_\star, \phi_\star)$ that maximize the log evidence averaged over the training set $\{x_1, \dots, x_M\}$:

$$\ell(\theta, \phi) := \frac{1}{M} \sum_{m=1}^M \log p_{\theta, \phi}(x_m), \quad \text{where} \quad p_{\theta, \phi}(x) := \int p_{\theta, \phi}(x, z_{0:K}) dz_{0:K} \quad (2)$$

denotes the probability density the model assigns to a given datapoint x . Assuming the training points are independent, this is equivalent to fitting the model through maximum likelihood.

Because the log-evidence is intractable, we instead consider the following lower bound:

$$-F(\theta, \phi, q^{1:M}) := \frac{1}{M} \sum_{m=1}^M \mathbb{E}_{q^m} \left[\log \frac{p_{\theta, \phi}(x, z_0)}{q^m(z_0)} \right] \leq \ell(\theta, \phi) \quad \forall (\theta, \phi, q^{1:M}) \in \Theta \times \Phi \times \mathcal{P}(\mathsf{Z})^M, \quad (3)$$

where $p_{\theta, \phi}(x, z_0) := \int p_{\theta, \phi}(x, z_{0:K}) dz_{1:K}$ and F denotes the *free energy*. Maximizing (3) above over all parameters θ, ϕ and M -tuples $q^{1:M} = (q^1, \dots, q^M)$ of distributions q^1, \dots, q^M over the latent

space is equivalent to maximizing $\ell(\theta, \phi)$ over all θ, ϕ ; see, e.g., [Neal and Hinton \(1998\)](#). However, $p_{\theta, \phi}(x, z_0)$ is intractable, and we must resort to one more lower bound:

$$-\tilde{F}(\theta, \phi, q^{1:M}) := \frac{1}{M} \sum_{m=1}^M \mathbb{E}_{q^m} \left[\log \frac{p_{\theta, \phi}(x, z_{0:K})}{q(z_{1:K}|z_0)q^m(z_0)} \right] \leq F(\theta, \phi, q^{1:M}) \leq \ell(\theta, \phi), \quad (4)$$

for all θ, ϕ , and $q^{1:M}$, where $q(z_{1:K}|z_0)$ denotes the *forward process*: a fixed user-chosen kernel as in DDPM. \tilde{F} amounts to a regularized version of F that penalizes deviations from the forward process:

$$\tilde{F} = F + \frac{1}{M} \sum_{m=1}^M \mathbb{E}_{q^m}[\mathcal{R}], \quad \text{where } \mathcal{R}(\theta, z_0) := D_{\text{KL}}(q(z_{1:K}|z_0) || p_{\theta}(z_{1:K}|z_0)), \quad (5)$$

where D_{KL} denotes the Kullback-Leibler divergence. Alternatively, we can view \tilde{F} as the free energy obtained replacing $p_{\theta, \phi}$ in (3) with the following *tilted* version:

$$\tilde{p}_{\theta, \phi}(x, z_0) := p_{\theta, \phi}(x, z_0) \exp(-\mathcal{R}(\theta, z_0)). \quad (6)$$

For this reason, similar arguments to those behind ([Neal and Hinton, 1998](#), Theorem 2) yield:

Proposition 2.1. (θ_*, ϕ_*) maximize $\tilde{\ell}(\theta, \phi) := M^{-1} \sum_{m=1}^M \log \tilde{p}_{\theta, \phi}(x_m)$ iff (θ_*, ϕ_*, q_*) minimize \tilde{F} for some q_* , where $\tilde{p}_{\theta, \phi}(x_m) := \int \tilde{p}_{\theta, \phi}(x, z_{0:K}) dz_{0:K}$.

Note that $\tilde{\ell}(\theta, \phi)$ in the above equals $\ell(\theta, \phi)$ in (2) whenever θ is such that the forward and reverse processes coincide (that is, when θ belongs to $\Theta_0 := \{\theta \in \Theta : \mathcal{R}(\theta, \cdot) \equiv 0\}$). Hence, if the θ -component of one of ℓ 's maximizers belongs to Θ_0 , it follows that ℓ and $\tilde{\ell}$ share the same maxima and maximizers, and Proposition 2.1 implies that the (θ, ϕ) -components of \tilde{F} 's minimizers maximize ℓ , our objective of interest. Because ℓ only depends on θ via $p_{\theta}(z_0) := \int p_{\theta}(z_{0:K}) dz_{1:K}$, a sufficient condition for the θ -component of one of ℓ 's maximizers to belong to Θ_0 is

$$\{p_{\theta}(z_0) : \theta \in \Theta\} = \{p_{\theta}(z_0) : \theta \in \Theta_0\}. \quad (7)$$

In practice, the above will not hold exactly (in fact, Θ_0 will be empty). However, we believe a close approximation is possible when the forward and reverse processes are chosen with care (generally, the more expressive the latter is, the better).

Previous works such as [Wehenkel and Louppe \(2021\)](#) restrict q^m to mean-field Gaussian distributions of the sort $\mathcal{N}(z_0; \mu_{\psi}(x^m), \Sigma_{\psi}(x^m))$, where the mean and (diagonal) covariance matrix are parametrized by an encoder with parameters ψ , and they optimize \tilde{F} over (θ, ϕ, ψ) . In the following, we take a different approach and replace these variational approximations with particle-based ones.

3 Methods

To obtain an algorithm for minimizing \tilde{F} in (4), we follow similar steps to those taken in [Kuntz et al. \(2023\)](#) to obtain particle-based algorithms for minimizing F in (3) for simpler latent variable models (in particular, ones for which $p_{\theta, \phi}(x, z_0)$ is tractable).

3.1 The gradient flow

To derive our algorithm, we search for an analogue of gradient descent (GD) applicable to \tilde{F} . GD for minimizing a function $f : \mathbb{R}^d \rightarrow \mathbb{R}$, $x_{k+1} = x_k - h \nabla_x f(x_k)$, is the Euler discretization with step size $h > 0$ of the continuous-time *gradient flow* $\dot{x}_t = -\nabla_x f(x_t)$. To obtain an analogue of GD applicable to \tilde{F} , we identify an appropriate analogue of the gradient flow and approximate it. The flow we consider features the gradient we obtain by endowing Φ and Θ with the Euclidean

geometry and $\mathcal{P}(\mathcal{Z})$ with the Wasserstein-2 one (see Appendix A.2 for details), in which case $\nabla \tilde{F} = (\nabla_\theta \tilde{F}, \nabla_\phi \tilde{F}, \nabla_{q^1} \tilde{F}, \dots, \nabla_{q^M} \tilde{F})$ where

$$\nabla_\theta \tilde{F}(\theta, \phi, q^{1:M}) = \frac{1}{M} \sum_{m=1}^M \mathbb{E}_{q^m(z_0)} [\nabla_\theta \mathcal{L}_D(\theta, z_0)], \quad (8)$$

$$\nabla_\phi \tilde{F}(\theta, \phi, q^{1:M}) = -\frac{1}{M} \sum_{m=1}^M \mathbb{E}_{q^m(z_0)} [\nabla_\phi \log p_\phi(x^m|z_0)], \quad (9)$$

$$\nabla_{q^m} \tilde{F}(\theta, \phi, q^{1:M}) = \nabla_{z_0} \cdot \left[q^m(z_0) \nabla_{z_0} \left[\log \left(\frac{p_\phi(x^m|z_0)}{q^m(z_0)} \right) - \mathcal{L}_D(\theta, z_0) \right] \right], \quad \forall m \in [M], \quad (10)$$

with $\mathcal{L}_D(\theta, z_0) := \mathbb{E}_{q(z_{1:K}|z_0)} \left[\log \frac{q(z_{1:K}|z_0)}{p_\theta(z_{0:K})} \right]$ denoting the *diffusion loss*, $\nabla \cdot$ the divergence operator, and $[M] := \{1, \dots, M\}$. The gradient flow then reads

$$(\dot{\theta}_t, \dot{\phi}_t, \dots, \dot{q}_t^{1:M}) = -\nabla \tilde{F}(\theta_t, \phi_t, q_t^{1:M}). \quad (11)$$

Using the results of Caprio et al. (2024), it is straightforward to obtain sufficient conditions under which the flow converges exponentially fast to \tilde{F} 's minimizers (see Appendix D for the proof):

Theorem 3.1. *Suppose that \mathcal{R} is strongly convex and $(\theta, \phi, x, z_0) \mapsto \log(p_{\theta, \phi}(x, z_0))$ is strongly concave, and that $\tilde{p}_{\theta, \phi}(x, z_0)$ satisfies the technical assumptions listed in Caprio et al. (2024, Assumptions 2, 3). Then, $\tilde{\ell}$ has a unique maximizer $(\theta_\star, \phi_\star)$ and the flow converges exponentially fast to it: for some $\lambda > 0$ independent of M ,*

$$\|(\theta_t, \phi_t) - (\theta_\star, \phi_\star)\| \leq \sqrt{\frac{2[\tilde{F}(\theta_t, \phi_t, q_t^{1:M}) - \tilde{F}_\star]}{\lambda}} \leq \sqrt{\frac{2[\tilde{F}(\theta_0, \phi_0, q_0^{1:M}) - \tilde{F}_\star]}{\lambda}} e^{-\lambda t}, \quad \forall t > 0;$$

where $\tilde{F}_\star := \inf_{(\theta, \phi, q^{1:M})} \tilde{F}(\theta, \phi, q^{1:M})$ and $\|\cdot\|$ denotes the Euclidean norm.

The strong convexity conditions in the theorem above can be relaxed and replaced with weaker ones, such as log-Sobolev inequalities (Caprio et al., 2024; Villani, 2003). In the interest of clarity, we do not pursue this here.

3.2 Approximating the flow and a simple algorithm

In almost all cases, (8–11) defines an intractable set of equations and we must approximate it. To do so, we exploit the fact (Kuntz et al., 2023, Section 2) that they form the Fokker-Planck equation satisfied by the law of the following McKean-Vlasov SDE (Chaintron and Diez, 2022):

$$d\theta_t = -\frac{1}{M} \sum_{m=1}^M \mathbb{E}_{q_t^m(z_0)} [\nabla_\theta \mathcal{L}_D(\theta_t, Z_{0,t}^m)] dt, \quad (12)$$

$$d\phi_t = \frac{1}{M} \sum_{m=1}^M \mathbb{E}_{q_t^m(z_0)} [\nabla_\phi \log p_{\phi_t}(x^m|Z_{0,t}^m)] dt, \quad (13)$$

$$dZ_{0,t}^m = \nabla_{z_0} [\log(p_{\phi_t}(x^m|Z_{0,t}^m)) - \mathcal{L}_D(\theta_t, Z_{0,t}^m)] dt + \sqrt{2} dW_t^m, \quad \forall m \in [M] \quad (14)$$

where q_t^m denotes the law of $Z_{0,t}^m$ and $(W_t^{1:M})_{t \geq 0}$ denotes a $d_z \times M$ -dimensional Brownian motion.

The laws $(q_t^{1:M})_{t \geq 0}$ are unknown and the continuous time axis intractable, so we must approximate the former and discretize the latter. In particular, we approximate the laws using the empirical distribution $N^{-1} \sum_{n=1}^N \delta_{Z_{0,t}^{1:M,n}}$ cloud of N weakly-dependent particles $Z_{0,t}^{1:M,1}, \dots, Z_{0,t}^{1:M,N}$ all (approximately) distributed according to $q_t^{1:M}$; and we discretize the time axis using the Euler-Maruyama

scheme:

$$\theta_{t+1} = \theta_t - \frac{h}{MN} \sum_{m=1}^M \sum_{i=1}^N \nabla_{\theta} \mathcal{L}_D(\theta_t, Z_{0,t}^{m,n}), \quad (15)$$

$$\phi_{t+1} = \phi_t + \frac{h}{MN} \sum_{m=1}^M \sum_{i=1}^N \nabla_{\phi} \log p_{\phi_t}(x^m | Z_{0,t}^{m,n}), \quad (16)$$

$$Z_{0,t+1}^{m,n} = Z_{0,t}^{m,n} + h \nabla_{z_0} [\log(p_{\phi_t}(x^m | Z_{0,t}^{m,n})) - \mathcal{L}_D(\theta_t, Z_{0,t}^{m,n})] + \sqrt{2h} W_t^{m,n}, \quad \forall n \in [N], m \in [M], \quad (17)$$

where $h > 0$ denotes the discretization step size, $W_{1:T}^{1:M,1:N}$ a $T \times M \times N$ -dimensional standard Gaussian random variable, and T denotes the total number of steps. Under the conditions in Theorem 3.1’s premise, and a further Lipschitz gradients assumption, it is straightforward to obtain error bounds for (15–17) using the results in Caprio et al. (2024):

Theorem 3.2. *Suppose that the premise of Theorem 3.1 holds, and that \mathcal{R} and $(\theta, \phi, x, z_0) \mapsto \log(p_{\theta, \phi}(x, z_0))$ have Lipschitz gradients. For all sufficiently small $h > 0$, there exists an $\mathcal{O}(h^{1/2} + N^{-1/2}) C_h^N$ independent of T , a $\rho \in (0, 1)$, and a $C > 0$ independent of (h, N, T) , such that*

$$\|(\theta_T, \phi_T) - (\theta_{\star}, \phi_{\star})\| \leq C_h^N + C\rho^T \quad \forall T = 0, 1, \dots,$$

where $(\theta_{\star}, \phi_{\star})$ denote $\tilde{\ell}$ unique maximizer.

In particular, the theorem shows the error can be made arbitrarily small by picking N, T sufficiently large and h sufficiently small.

3.3 A practical algorithm: IPLD

While amenable to theoretical analysis, the algorithm defined by (15–17) performs poorly in practice when applied to models of the sort we are interested in for several reasons. We deal with these one at a time and obtain a practical version well-suited to modern computing environments.

Subsampling. The updates in (15–17) incur a $\mathcal{O}(NMK)$ computational cost, which proves prohibitively expensive for all but the smallest of training sets. We overcome this issue by subsampling similarly as in Welling and Teh (2011); Ho et al. (2020). First, we rewrite (15–17) more concisely as

$$\begin{aligned} (\theta_{t+1}, \phi_{t+1}) &= (\theta_t, \phi_t) - h \nabla_{(\theta, \phi)} \mathcal{L}(\theta_t, \phi_t, Z_{0,t}^{1:M,1:N}), \\ Z_{0,t+1}^{1:M,1:N} &= Z_{0,t}^{1:M,1:N} - h \nabla_{z_0^{1:M,1:N}} \mathcal{L}(\theta_t, \phi_t, Z_{0,t}^{1:M,1:N}) + \sqrt{2h} W_t^{1:M,1:N}, \end{aligned}$$

where $\mathcal{L}(\theta, \phi, z_0^{1:M,1:N}) := (MN)^{-1} \sum_{m=1}^M \sum_{n=1}^N [\mathcal{L}_D(\theta, z_0^{m,n}) - \log p_{\phi}(x_m | z_{0,t}^{m,n})]$. Then, we replace the loss \mathcal{L} with the following unbiased estimate:

$$\hat{\mathcal{L}}(\theta_t, \phi_t, z_{0,t}^{1:M,1:N}) := \frac{1}{N|\mathcal{B}|} \sum_{(m,n) \in \mathcal{B} \times [N]} \left[\hat{\mathcal{L}}_D(\theta_t, z_{0,t}^{m,n}) - \log p_{\phi}(x_m | z_{0,t}^{m,n}) \right], \quad (18)$$

where \mathcal{B} denotes a subset of $[M]$ of size $|\mathcal{B}|$ drawn uniformly at random (and independently of all other random variables), and $\hat{\mathcal{L}}_D$ denotes the $\mathcal{O}(1)$ -cost unbiased estimate of the diffusion loss \mathcal{L}_D specified in Appendix A.1; so bringing down the cost to $\mathcal{O}(N|\mathcal{B}|)$. See Algorithm 1 for pseudocode.

Distributed Training. (15–17) require $\mathcal{O}(MN)$ memory. However, IPLD is well-suited for distributed training: $Z_{0,t}^{m,n}$ ’s update for a given pair (m, n) is independent of that for all other pairs, and requires only access to the m th datapoint. Thus, in distributed setups, we allocate each accelerator a disjoint subset of the training set and it handles the corresponding updates for all N particles; so making the per-device memory cost proportional to only the size of the corresponding subset. The communication costs are also reduced, as we need not synchronize the z -gradients. This contrasts with autoencoder-based LDMS that necessitate synchronizing gradients for encoders (typically, deep networks) when trained end-to-end.

Algorithm 1 IPLD

```
1: Inputs: Dataset  $\{x_m\}_{m \in [M]}$ , stepsize  $h$ ,  
2: particles  $z_{0,0}^{1:M,1:N}$ , parameters  $\phi, \theta$   
3: while not converged do  
4:   Sample a mini-batch of indices  $\mathcal{B} \subset [M]$   
5:   Compute  $\hat{\mathcal{L}}_t = \hat{\mathcal{L}}(\theta_t, \phi_t, z_{0,t}^{1:M,1:N})$  in (18)  
6:   for  $(m, n) \in [M] \times [N]$  do  
7:     if  $m \in \mathcal{B}$  then  
8:        $z_{0,t}^{m,n} \leftarrow z_{0,t}^{m,n} - Nh \nabla_{z_0}^{m,n} \hat{\mathcal{L}}_t$   
9:     end if  
10:     $z_{0,t+1}^{m,n} \leftarrow z_{0,t}^{m,n} + \sqrt{\frac{2h}{M}} W_t^{m,n}$   
11:  end for  
12:   $\theta_{t+1} \leftarrow \theta_t - h \nabla_{\theta} \hat{\mathcal{L}}_t$   
13:   $\phi_{t+1} \leftarrow \phi_t - h \nabla_{\phi} \hat{\mathcal{L}}_t$   
14: end while  
15: Outputs:  $(\theta_t, \phi_t, z_{0,t}^{1:M,1:N})$ 
```

We provide the pseudocode for the full training algorithm in Appendix A.4.

Reweighting and annealing. We re-weight the diffusion loss $\mathcal{L}_{\mathcal{D}}$ similarly as in Ho et al. (2020), as this re-weighting is known to improve sample quality (Song et al., 2021b; Kingma and Gao, 2023); see Appendix A.1 for details. Furthermore, we anneal the KL term in the free-energy (3):

$$\tilde{F}(\theta, \phi, q^{1:M}) = \frac{1}{M} \sum_{m=1}^M \left(\underbrace{-\mathbb{E}_{q^m} [\log p_{\phi}(x|z_0)]}_{\text{Reconstruction}} + \gamma_t \underbrace{D_{\text{KL}}(q^m(z_0) || p_{\theta}(z_0))}_{\text{Diffusion prior regularizer}} \right),$$

where $\gamma_t : [0, \infty) \rightarrow (0, \infty)$ denotes the (non-decreasing) annealing schedule. This is a practice commonly used when training deep Latent Variable Models (LVMs) to encourage accurate reconstruction during the early stages of training (Sønderby et al., 2016; Fu et al., 2019; Vahdat and Kautz, 2020; Vahdat et al., 2021). Adjusting \tilde{F} correspondingly results in γ_t pre-multiplying $\mathcal{L}_{\mathcal{D}}$ in (10); which in turn corresponds to adjusting the noise levels in (14,17) by replacing $\sqrt{2h}$ therein with $\sqrt{2h\gamma_t}$ (cf. Appendix A.4.1 for details).

4 Related Work

Interacting Particle Algorithms. Interacting particle systems have long been the foundation of much statistical and optimization methodology, e.g. (Del Moral, 2004; Kennedy and Eberhart, 1995). Their use in algorithms that fit latent variable models by jointly updating model’s parameters and a latent-space particle cloud to maximize the likelihood is more recent: Kuntz et al. (2023) proposed several such algorithms and Lim et al. (2024) improved their performance by incorporating momentum into the algorithms’ updates (see also Encinar et al. (2024); Sharrock et al. (2024); Oliva and Akyildiz (2024); Marion et al. (2025); Akyildiz et al. (2025)). The theoretical guarantees of our algorithm are derived from the results in Caprio et al. (2024). Similar error bounds have been established in Akyildiz et al. (2025) for an alternative approximation to the gradient flow featuring noise in the parameter updates. Also related to our method are numerous works approximating gradient flows with particles to obtain alternatives to conventional Variational Inference (VI); e.g., Liu and Wang (2016); Lambert et al. (2022); Duncan et al. (2023); Diao et al. (2023); Lim and Johansen (2024). Lastly, there is a growing body of work exploring training methodologies for generative models in the ambient space using particle-based methods (Arbel et al., 2019; Yi et al., 2023; Franceschi et al., 2023; Galashov et al., 2024; Zhou et al., 2025).

Preconditioning and momentum. When training simpler latent variable models with algorithms similar to ours, Kuntz et al. (2023); Lim et al. (2024) observed that preconditioning the models’ parameters similarly as in RMSProp (Tieleman and Hinton, 2012) mitigated ill-conditioning and stabilized the training. Lim et al. (2024) further noted gains in both training speeds and test-time performance by incorporating momentum into the parameter and particle updates. Here we precondition and incorporate momentum for both the parameters and particles. We use optimizers like AdamW (Loshchilov and Hutter, 2019) for the former and adaptive Langevin algorithms (Li et al., 2016; Kim et al., 2020) for the latter. Lastly, we choose different step sizes h_{θ} , h_{ϕ} , and h_z respectively for θ , ϕ , and the particles to account for the multi-scale nature of the interacting particle system (Akyildiz et al., 2024; Pavliotis and Stuart, 2008).

Latent Diffusion Models. There have been many attempts at incorporating DMs into LVMs as the prior $p_\theta(z)$. Vahdat et al. (2021) proposed to jointly train a continuous-time score-based DM (Song et al., 2021c) in the latent space of a deep hierarchical VAE (Vahdat and Kautz, 2020). Similarly, Wehenkel and Louppe (2021) considered the joint training of a discrete-time DM with a conventional VAE. Cohen et al. (2022) instead applied a discrete-time diffusion prior to a Vector-Quantised Variational Autoencoder (VQ-VAE) (van den Oord et al., 2017). The seminal work by Rombach et al. (2022) can also be viewed as learning a diffusion prior post training of the VAE. Concurrent to our work, Leng et al. (2025) also considers the joint training of a latent diffusion model with the VAE, but their objective is based instead on the REPresentation Alignment (REPA) loss (Yu et al., 2025). Additionally, several studies have proposed a trainable forward process for diffusion models (Kim et al., 2022; Bartosh et al., 2024a,b; Nielsen et al., 2024), which can be viewed as generalizations of latent diffusion models. More recently, combinations of diffusion-based priors with other types of probabilistic models in hierarchical VAEs have been explored, such as Energy-based Model (EBM) (Cui and Han, 2024) and Variational Mixture of Posteriors prior (Kuzina and Tomczak, 2024). Additionally, the work by Silvestri et al. (2025) can also be viewed as an VAE with a consistency model (Song et al., 2023) learning the aggregated posterior.

Decoder-only Models. Connected to our work other methods that, similarly to us, optimize latent variables rather than relying on an encoder network. Several studies (Han et al., 2017; Nijkamp et al., 2019, 2020; Pang et al., 2020; Nijkamp et al., 2022; Yu et al., 2023) have considered short-run and persistent Langevin dynamics within an Expectation-Maximisation (EM) framework to train latent variable models featuring a “generator” network. Similarly, Generative Latent Optimization (Bojanowski et al., 2018), while originally proposed as an alternative to the adversarial training of Generative Adversarial Networks (GANs) (Goodfellow et al., 2014), can also be interpreted as an approach that directly optimizes the latent variables with gradient descent.

5 Experiments

We evaluate IPLD’s performance on two synthetic datasets (Section 5.1) and three image datasets (Section 5.2). In the synthetic case, we benchmark against the closest VI analogue to IPLD we have been able to locate in the literature: VAE with a Diffusion Prior (DIFFUSIONVAE) (Wehenkel and Louppe, 2021); see the end of Section 2 for more details. For the image datasets, we additionally compare with several other decoder-only LVM (cf. Section 4).

5.1 Synthetic Datasets

We first validate the effectiveness of our method on two toy datasets. We generate these by first sampling from a distribution on a 2-dimensional latent space, and then mapping the samples into a 64-dimensional ambient space using a matrix $A \in \mathbb{R}^{2 \times 64}$ with orthogonal rows. We consider 1) a Gaussian Mixture Model (GMM) with 25 components as in Boys et al. (2024); Cardoso et al. (2024), and 2) a distribution concentrated on concentric circles similar to that¹ in `scikit-learn`. We train both DIFFUSIONVAE and IPLD for 1,000 steps and varying numbers of particles $N = 1, 4, 16, 64, 256$ (in the case of DIFFUSIONVAE, N refers to the number of samples drawn from the encoder at each step). For both datasets, increasing N increases the quality of the samples generated by IPLD (Figure 2). To quantitatively compare IPLD and DIFFUSIONVAE, we estimate

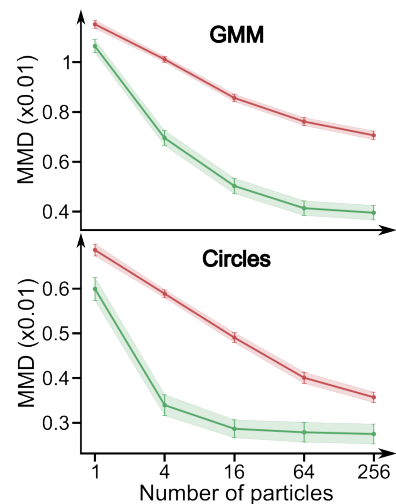


Figure 1: Estimated MMD between the ground truth and the distribution learned with IPLD (green) and DiffusionVAE (red) for the GMM (top) and concentric circles (bottom) datasets.

¹https://scikit-learn.org/stable/modules/generated/sklearn.datasets.make_circles.html

the Maximum Mean Discrepancy (MMD) (Gretton et al., 2012) between the distribution learned by each and the ground truth. The MMD values are averaged over 50 training runs and the standard error is reported. For all particle numbers, IPLD outperformed DIFFUSIONVAE (Figure 1). See Appendix B.1 for more details.

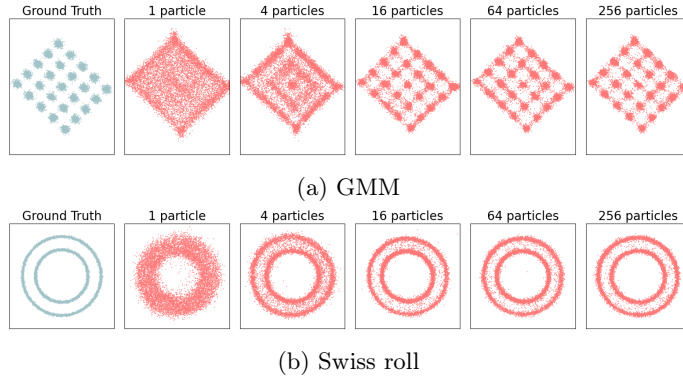


Figure 2: Samples generated by IPLD trained with varying numbers of particles for 1,000 steps (first two components out of the $d_x = 64$ many).

5.2 Image Modelling

Next, we test our model on three image datasets: CIFAR-10 (Krizhevsky and Hinton, 2009), SVHN (Netzer et al., 2011), and CelebA64 (Liu et al., 2015). As before, we benchmark against DIFFUSIONVAE using the same decoder, diffusion model, and $4 \times 8 \times 8$ -dimensional latent space as for IPLD. We train both models for the same number of epochs (400 for CIFAR10 and SVHN, 200 for CelebA64); see Appendix B.2 for details. For IPLD, we vary the particle number $N = 1, 5, 10$ (we use a single particle for DIFFUSIONVAE because back-propagating the corresponding gradients through the model’s encoder with more particles proved too memory-consuming for our hardware). We warm-start the multi-particle IPLD runs using a single particle as in Kuntz et al. (2023); see Appendix B.3 for details. In both cases, we compute Fréchet Inception Distance (FID) scores for the trained model (Table 1). IPLD outperforms DIFFUSIONVAE, and its performance increases with the number of particles used for training. IPLD also proves competitive with previous decoder-only models discussed in Section 4 (see also Table 1).

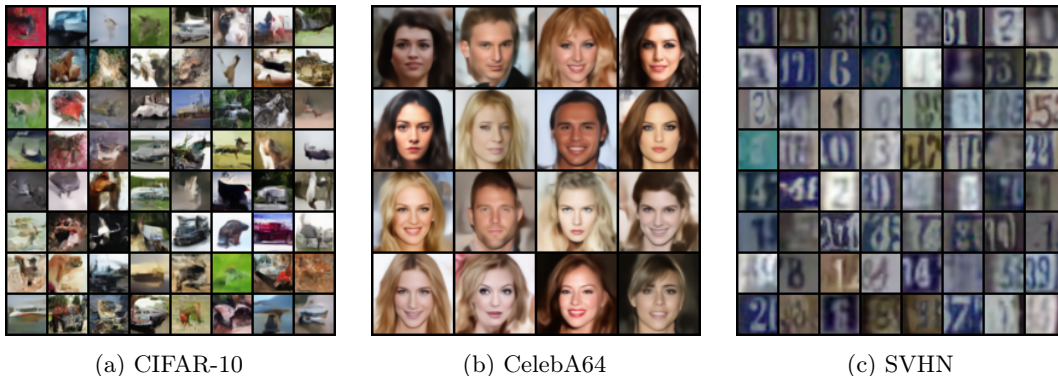


Figure 3: Samples generated with IPLD trained on CIFAR-10, CelebA64, and SVHN. The CelebA64 samples have been curated for better visualization. See Appendix C.3 for additional samples (including uncurated CelebA64 ones).

Models	FID↓	Models	FID↓
Decoder-only LVMs		DAMC (Yu et al., 2023)	30.83
PGD (Kuntz et al., 2023)	101.4	LP-EBM (Pang et al., 2020)	37.87
MPGD (Lim et al., 2024)	91.7	EBM-SR (Nijkamp et al., 2019)	23.03
DAMC (Yu et al., 2023)	57.72	DiffusionVAE (Wehenkel and Louppe, 2021)	67.95
LP-EBM (Pang et al., 2020)	70.15	DiffusionVAE*	29.24
EBM-SR (Nijkamp et al., 2019)	44.50	Ours	
VAE		IPLD (1 particle)	22.86
DiffusionVAE (Wehenkel and Louppe, 2021)	153.1	IPLD (5 particles)	21.55
DiffusionVAE*	62.07	IPLD (10 particles)	21.43
Ours		(b) FID(↓) of models trained on CelebA64.	
IPLD (1 particle)	51.60	Models	FID↓
IPLD (5 particles)	48.30	DAMC (Yu et al., 2023)	18.76
IPLD (10 particles)	46.95	LP-EBM (Pang et al., 2020)	29.44
(a) FID(↓) of models trained on CIFAR-10.		DiffusionVAE* (Wehenkel and Louppe, 2021)	20.89
We report both the original results from Wehenkel and Louppe (2021) and our re-implementation (denoted by "*") of the DIFFUSIONVAE using the same architecture (see Appendix B).		Ours	
		IPLD (1 particle)	17.55
		IPLD (5 particles)	14.02
		IPLD (10 particles)	13.51
		(c) FID(↓) of models trained on SVHN.	

Table 1: FID scores for CIFAR-10, SVHN, and CelebA64 estimated using 50,000 samples.

6 Discussion

Like many before us, we recast fitting an LDM via maximum likelihood as minimizing a free energy functional (Section 2). Unlike others, we then identify a gradient flow that minimizes the functional and approximate it using systems of interacting particles (Sections 3.1, 3.2), and we theoretically characterize both the flow and the approximations (Theorems 3.1, 3.2) under standard assumptions. Following these steps, we obtain IPLD (Section 3.3): a theoretically-principled algorithm for end-to-end LDM training. Because it entails updating a cloud of particles and each particle’s update is independent of the others’, IPLD is well-suited for modern distributed compute environments and is easy to scale.

In numerical experiments involving both synthetic and image data, IPLD compares favorably with relevant benchmarks (Section 5). However, our results on the image dataset fall short of today’s state-of-the-art. We believe this may be due to the relatively small latent spaces, decoder, and DM architectures we use (e.g., compare Appendix B.2 with Vahdat et al. (2021, Appendices G.1,2)) and our limited computational budget (e.g., compare Appendix B.4 with Rombach et al. (2022, Appendix E)), rather than a fundamental limitation of the approach.

Our work may be limited by the fact that, to date, LDMs trained in a two-stage manner (e.g., Rombach et al. (2022)) have achieved results that those trained end-to-end have not, and our approach is fundamentally an end-to-end one. However, recent works such as Leng et al. (2025) have demonstrated promising breakthroughs in end-to-end LDM training, and their innovations are relatively straightforward to incorporate in our algorithm. Further improvements may be possible through more careful subsampling schemes than that in Section 3.3 and the use of variance reduction techniques (Zou et al., 2018). Indeed, we hope our work paves the way to other more effective particle-based algorithms for LDM training.

Lastly, our theoretical analysis is limited to the simplified algorithm in Section 3.2. However, we believe that it be possible to extend the analysis to more practical versions using techniques along the lines of those used to study adaptive optimizers (Malladi et al., 2022) and momentum-enriched interacting particle systems (Oliva and Akyildiz, 2024; Lim et al., 2024).

Societal Impacts. We provide novel training algorithms for LDMs and the potential societal impacts of our work largely follow those of this sort deep generative model. Problematic ones include

the generation of “deep fakes”, enabling misinformation and propaganda, and exacerbating biases in the training data; see [Rombach et al. \(2022\)](#)’s impact statement for a longer discussion and pertinent references. There are, however, many positive potential impacts ranging from enabling creative applications to facilitating therapeutic development ([Watson et al., 2023](#)).

References

- Akyildiz, Ö. D., Crucinio, F. R., Girolami, M., Johnston, T., and Sabanis, S. (2025). Interacting particle Langevin algorithm for maximum marginal likelihood estimation. *ESAIM: Probability and Statistics*.
- Akyildiz, O. D., Ottobre, M., and Souttar, I. (2024). A multiscale perspective on maximum marginal likelihood estimation. *arXiv preprint arXiv:2406.04187*.
- Ambrosio, L., Brué, E., Semola, D., et al. (2021). *Lectures on optimal transport*, volume 130. Springer.
- Arbel, M., Korba, A., SALIM, A., and Gretton, A. (2019). Maximum mean discrepancy gradient flow. In *Advances in Neural Information Processing Systems*, volume 32.
- Bartosh, G., Vetrov, D., and Naesseth, C. A. (2024a). Neural diffusion models. In *Forty-first International Conference on Machine Learning*.
- Bartosh, G., Vetrov, D., and Naesseth, C. A. (2024b). Neural flow diffusion models: Learnable forward process for improved diffusion modelling. In *The Thirty-eighth Annual Conference on Neural Information Processing Systems*.
- Bojanowski, P., Joulin, A., Lopez-Pas, D., and Szlam, A. (2018). Optimizing the latent space of generative networks. In *International Conference on Machine Learning*. PMLR.
- Boys, B., Girolami, M., Pidstrigach, J., Reich, S., Mosca, A., and Akyildiz, O. D. (2024). Tweedie moment projected diffusions for inverse problems. *Transactions on Machine Learning Research*. Featured Certification.
- Buitinck, L., Louppe, G., Blondel, M., Pedregosa, F., Mueller, A., Grisel, O., Niculae, V., Prettenhofer, P., Gramfort, A., Grobler, J., Layton, R., VanderPlas, J., Joly, A., Holt, B., and Varoquaux, G. (2013). API design for machine learning software: experiences from the scikit-learn project. In *ECML PKDD Workshop: Languages for Data Mining and Machine Learning*.
- Caprio, R., Kuntz, J., Power, S., and Johansen, A. M. (2024). Error bounds for particle gradient descent, and extensions of the log-sobolev and talagrand inequalities. *arXiv preprint arXiv:2403.02004*.
- Cardoso, G., el idrissi, Y. J., Corff, S. L., and Moulines, E. (2024). Monte carlo guided denoising diffusion models for bayesian linear inverse problems. In *The Twelfth International Conference on Learning Representations*.
- Chaintron, L.-P. and Diez, A. (2022). Propagation of chaos: A review of models, methods and applications. i. models and methods. *Kinetic and Related Models*, 15(6):895.
- Cohen, M., Quispe, G., Corff, S. L., Ollion, C., and Moulines, E. (2022). Diffusion bridges vector quantized variational autoencoders. In *Proceedings of the 39th International Conference on Machine Learning*, volume 162 of *Proceedings of Machine Learning Research*.
- Cui, J. and Han, T. (2024). Learning latent space hierarchical EBM diffusion models. In *Proceedings of the 41st International Conference on Machine Learning*, volume 235 of *Proceedings of Machine Learning Research*.
- Del Moral, P. (2004). *Feynman-Kac Formulae: Genealogical and Interacting Particle Systems with Applications*. Springer.

- Dhariwal, P. and Nichol, A. Q. (2021). Diffusion models beat GANs on image synthesis. In *Advances in Neural Information Processing Systems*.
- Diao, M. Z., Balasubramanian, K., Chewi, S., and Salim, A. (2023). Forward-backward gaussian variational inference via jko in the bures-wasserstein space. In *International Conference on Machine Learning*, pages 7960–7991. PMLR.
- Dieleman, S. (2025). Generative modelling in latent space.
- Duncan, A., Nuesken, N., and Szpruch, L. (2023). On the geometry of stein variational gradient descent. *Journal of Machine Learning Research*, 24(56):1–39.
- Efron, B. (2011). Tweedie’s formula and selection bias. *Journal of the American Statistical Association*, 106(496):1602–1614.
- Encinar, P. C., Crucinio, F. R., and Akyildiz, O. D. (2024). Proximal interacting particle langevin algorithms. *arXiv preprint arXiv:2406.14292*.
- Franceschi, J.-Y., Gartrell, M., Santos, L. D., Issenhuth, T., de Bezenac, E., Chen, M., and Rakotomamonjy, A. (2023). Unifying GANs and score-based diffusion as generative particle models. In *Thirty-Seventh Conference on Neural Information Processing Systems*.
- Fu, H., Li, C., Liu, X., Gao, J., Celikyilmaz, A., and Carin, L. (2019). Cyclical annealing schedule: A simple approach to mitigating kl vanishing. *North American Chapter of the Association for Computational Linguistics*.
- Galashov, A., de Bortoli, V., and Gretton, A. (2024). Deep MMD gradient flow without adversarial training. *arXiv preprint arXiv:2405.06780*.
- Goodfellow, I. J., Pouget-Abadie, J., Mirza, M., Xu, B., Warde-Farley, D., Ozair, S., Courville, A., and Bengio, Y. (2014). Generative adversarial nets. In *Advances in Neural Information Processing Systems*, volume 27.
- Gretton, A., Borgwardt, K. M., Rasch, M. J., Schölkopf, B., and Smola, A. (2012). A kernel two-sample test. *Journal of Machine Learning Research*, 13(25):723–773.
- Han, T., Lu, Y., Zhu, S.-C., and Wu, Y. N. (2017). Alternating back-propagation for generator network. In *Proceedings of the Thirty-First AAAI Conference on Artificial Intelligence*, AAAI’17.
- Heusel, M., Ramsauer, H., Unterthiner, T., Nessler, B., and Hochreiter, S. (2017). Gans trained by a two time-scale update rule converge to a local nash equilibrium. In *Proceedings of the 31st International Conference on Neural Information Processing Systems*, NIPS’17.
- Ho, J., Jain, A., and Abbeel, P. (2020). Denoising diffusion probabilistic models. In *Advances in Neural Information Processing Systems*, volume 33.
- Huang, Y.-J. and Zhang, Y. (2023). GANs as gradient flows that converge. *Journal of Machine Learning Research*, 24(217):1–40.
- Kennedy, J. and Eberhart, R. (1995). Particle swarm optimization. In *Proceedings of ICNN’95 - International Conference on Neural Networks*, volume 4.
- Kim, D., Na, B., Kwon, S. J., Lee, D., Kang, W., and chul Moon, I. (2022). Maximum likelihood training of implicit nonlinear diffusion model. In *Advances in Neural Information Processing Systems*.
- Kim, S., Song, Q., and Liang, F. (2020). Stochastic gradient langevin dynamics algorithms with adaptive drifts. *arXiv preprint arXiv:2009.09535*.
- Kingma, D. P. and Ba, J. (2014). Adam: A method for stochastic optimization. *International Conference on Learning Representations*.

- Kingma, D. P. and Gao, R. (2023). Understanding diffusion objectives as the ELBO with simple data augmentation. In *Thirty-seventh Conference on Neural Information Processing Systems*.
- Kingma, D. P. and Welling, M. (2013). Auto-encoding variational bayes. *CoRR*, abs/1312.6114.
- Krizhevsky, A. and Hinton, G. (2009). Learning multiple layers of features from tiny images. Technical Report 0, University of Toronto, Toronto, Ontario.
- Kuntz, J., Lim, J. N., and Johansen, A. M. (2023). Particle algorithms for maximum likelihood training of latent variable models. In *Proceedings of The 26th International Conference on Artificial Intelligence and Statistics*, volume 206 of *Proceedings of Machine Learning Research*.
- Kuzina, A. and Tomczak, J. M. (2024). Hierarchical VAE with a diffusion-based vampprior. *Transactions on Machine Learning Research*.
- Lambert, M., Chewi, S., Bach, F., Bonnabel, S., and Rigollet, P. (2022). Variational inference via wasserstein gradient flows. In Oh, A. H., Agarwal, A., Belgrave, D., and Cho, K., editors, *Advances in Neural Information Processing Systems*.
- Lee, J. M. (2018). *Introduction to Riemannian Manifolds*, volume 176 of *Graduate Texts in Mathematics*. Springer.
- Leng, X., Singh, J., Hou, Y., Xing, Z., Xie, S., and Zheng, L. (2025). Repa-e: Unlocking vae for end-to-end tuning with latent diffusion transformers. *arXiv preprint arXiv:2504.10483*.
- Li, C., Chen, C., Carlson, D., and Carin, L. (2016). Preconditioned stochastic gradient langevin dynamics for deep neural networks. In *AAAI*.
- Lim, J. N. and Johansen, A. M. (2024). Particle semi-implicit variational inference. *Neural Information Processing Systems*.
- Lim, J. N., Kuntz, J., Power, S., and Johansen, A. M. (2024). Momentum particle maximum likelihood. In *Forty-First International Conference on Machine Learning*.
- Liu, Q. and Wang, D. (2016). Stein variational gradient descent: A general purpose bayesian inference algorithm. In *Advances in Neural Information Processing Systems*, volume 29.
- Liu, Z., Luo, P., Wang, X., and Tang, X. (2015). Deep learning face attributes in the wild. In *Proceedings of International Conference on Computer Vision (ICCV)*.
- Loshchilov, I. and Hutter, F. (2019). Decoupled weight decay regularization. *arXiv preprint arXiv:1711.05101*.
- Malladi, S., Lyu, K., Panigrahi, A., and Arora, S. (2022). On the SDEs and scaling rules for adaptive gradient algorithms. In Oh, A. H., Agarwal, A., Belgrave, D., and Cho, K., editors, *Advances in Neural Information Processing Systems*.
- Marion, P., Korba, A., Bartlett, P., Blondel, M., Bortoli, V. D., Doucet, A., Llinares-López, F., Paquette, C., and Berthet, Q. (2025). Implicit diffusion: Efficient optimization through stochastic sampling. *arXiv preprint arXiv:2402.05468*.
- Neal, R. M. and Hinton, G. E. (1998). *A View of the Em Algorithm that Justifies Incremental, Sparse, and other Variants*, pages 355–368. Springer Netherlands, Dordrecht.
- Netzer, Y., Wang, T., Coates, A., Bissacco, A., Wu, B., and Ng, A. Y. (2011). Reading digits in natural images with unsupervised feature learning. In *NIPS Workshop on Deep Learning and Unsupervised Feature Learning 2011*.
- Nie, S., Zhu, F., You, Z., Zhang, X., Ou, J., Hu, J., Zhou, J., Lin, Y., Wen, J.-R., and Li, C. (2025). Large language diffusion models. *arXiv preprint arXiv:2502.09992*.

- Nielsen, B. M. G., Christensen, A., Dittadi, A., and Winther, O. (2024). Diffenc: Variational diffusion with a learned encoder. In *The Twelfth International Conference on Learning Representations*.
- Nijkamp, E., Gao, R., Sountsov, P., Vasudevan, S., Pang, B., Zhu, S.-C., and Wu, Y. N. (2022). MCMC should mix: Learning energy-based model with neural transport latent space MCMC. In *International Conference on Learning Representations*.
- Nijkamp, E., Hill, M., Zhu, S.-C., and Wu, Y. N. (2019). Learning non-convergent non-persistent short-run MCMC toward energy-based model. In *Advances in Neural Information Processing Systems*, volume 32.
- Nijkamp, E., Pang, B., Han, T., Zhu, S.-C., and Wu, Y. N. (2020). Learning multi-layer latent variable model via variational optimization of short run mcmc for approximate inference. *ECCV*.
- Oliva, P. F. V. and Akyildiz, O. D. (2024). Kinetic interacting particle langevin monte carlo. *arXiv preprint arXiv:2407.05790*.
- Otto, F. (2001). The geometry of dissipative evolution equations: The porous medium equation. *Communications in Partial Differential Equations*, 26(1-2):101–174.
- Pang, B., Han, T., Nijkamp, E., Zhu, S.-C., and Wu, Y. N. (2020). Learning latent space energy-based prior model. In *Advances in Neural Information Processing Systems*, volume 33.
- Pavliotis, G. A. and Stuart, A. M. (2008). *Averaging for ODEs and SDEs*, pages 145–156. Springer New York, New York, NY.
- Peebles, W. and Xie, S. (2023). Scalable diffusion models with transformers. In *Proceedings of the IEEE/CVF International Conference on Computer Vision (ICCV)*.
- Podell, D., English, Z., Lacey, K., Blattmann, A., Dockhorn, T., Müller, J., Penna, J., and Rombach, R. (2024). SDXL: Improving latent diffusion models for high-resolution image synthesis. In *The Twelfth International Conference on Learning Representations*.
- Rombach, R., Blattmann, A., Lorenz, D., Esser, P., and Ommer, B. (2022). High-resolution image synthesis with latent diffusion models. In *Proceedings of the IEEE/CVF Conference on Computer Vision and Pattern Recognition (CVPR)*.
- Saxe, A. M., McClelland, J. L., and Ganguli, S. (2014). Exact solutions to the nonlinear dynamics of learning in deep linear neural networks.
- Sharrock, L., Dodd, D., and Nemeth, C. (2024). Tuning-free maximum likelihood training of latent variable models via coin betting. In *Proceedings of The 27th International Conference on Artificial Intelligence and Statistics*.
- Silvestri, G., Ambrogioni, L., Lai, C.-H., Takida, Y., and Mitsufuji, Y. (2025). Training consistency models with variational noise coupling. *arXiv preprint arXiv:2502.18197*.
- Sohl-Dickstein, J., Weiss, E., Maheswaranathan, N., and Ganguli, S. (2015). Deep unsupervised learning using nonequilibrium thermodynamics. In *Proceedings of the 32nd International Conference on Machine Learning*, volume 37 of *Proceedings of Machine Learning Research*.
- Sønderby, C. K., Raiko, T., Maaløe, L., Sønderby, S. K., and Winther, O. (2016). Ladder variational autoencoders. In *Advances in Neural Information Processing Systems*, volume 29.
- Song, J., Meng, C., and Ermon, S. (2021a). Denoising diffusion implicit models. In *International Conference on Learning Representations*.
- Song, Y., Dhariwal, P., Chen, M., and Sutskever, I. (2023). Consistency models. *International Conference on Machine Learning*.

- Song, Y., Durkan, C., Murray, I., and Ermon, S. (2021b). Maximum likelihood training of score-based diffusion models. *arXiv preprint arXiv:2101.09258*, pages 1415–1428.
- Song, Y. and Ermon, S. (2020). Improved techniques for training score-based generative models. In *Advances in Neural Information Processing Systems 33: Annual Conference on Neural Information Processing Systems 2020, NeurIPS 2020, December 6-12, 2020, virtual*.
- Song, Y., Sohl-Dickstein, J., Kingma, D. P., Kumar, A., Ermon, S., and Poole, B. (2021c). Score-based generative modeling through stochastic differential equations. In *International Conference on Learning Representations*.
- Tieleman, T. and Hinton, G. (2012). Lecture 6.5-rmsprop, coursera: Neural networks for machine learning. *University of Toronto, Technical Report*, 6.
- Vahdat, A. and Kautz, J. (2020). Nvae: A deep hierarchical variational autoencoder. In Larochelle, H., Ranzato, M., Hadsell, R., Balcan, M., and Lin, H., editors, *Advances in Neural Information Processing Systems*, volume 33.
- Vahdat, A., Kreis, K., and Kautz, J. (2021). Score-based generative modeling in latent space. In *Advances in Neural Information Processing Systems*, volume 34.
- van den Oord, A., Vinyals, O., and Kavukcuoglu, K. (2017). Neural discrete representation learning. In *Advances in Neural Information Processing Systems*, volume 30.
- Villani, C. (2003). *Topics in optimal transportation*. Graduate studies in mathematics ; v. 58. American Mathematical Society, Providence, RI.
- Villani, C. et al. (2008). *Optimal transport: old and new*, volume 338. Springer.
- Watson, J. L., Juergens, D., Bennett, N. R., Trippe, B. L., Yim, J., Eisenach, H. E., Ahern, W., Borst, A. J., Ragotte, R. J., Milles, L. F., Wicky, B. I. M., Hanikel, N., Pellock, S. J., Courbet, A., Sheffler, W., Wang, J., Venkatesh, P., Sappington, I., Torres, S. V., Lauko, A., De Bortoli, V., Mathieu, E., Ovchinnikov, S., Barzilay, R., Jaakkola, T. S., DiMaio, F., Baek, M., and Baker, D. (2023). De novo design of protein structure and function with RFdiffusion. *Nature*, 620(7976):1089–1100.
- Wehenkel, A. and Louppe, G. (2021). Diffusion priors in variational autoencoders. In *ICML Workshop on Invertible Neural Networks, Normalizing Flows, and Explicit Likelihood Models*.
- Welling, M. and Teh, Y. W. (2011). Bayesian learning via stochastic gradient langevin dynamics. In *Proceedings of the 28th International Conference on International Conference on Machine Learning, ICML’11*.
- Yi, M., Zhu, Z., and Liu, S. (2023). Monoflow: Rethinking divergence gans via the perspective of wasserstein gradient flows. *International Conference on Machine Learning*.
- Yu, P., Zhu, Y., Xie, S., Ma, X., Gao, R., Zhu, S.-C., and Wu, Y. N. (2023). Learning energy-based prior model with diffusion-amortized MCMC. In *Thirty-seventh Conference on Neural Information Processing Systems*.
- Yu, S., Kwak, S., Jang, H., Jeong, J., Huang, J., Shin, J., and Xie, S. (2025). Representation alignment for generation: Training diffusion transformers is easier than you think. In *The Thirteenth International Conference on Learning Representations*.
- Zhou, L., Ermon, S., and Song, J. (2025). Inductive moment matching. *arXiv preprint arXiv:2503.07565*.
- Zou, D., Xu, P., and Gu, Q. (2018). Subsampled stochastic variance-reduced gradient langevin dynamics. In *34th Conference on Uncertainty in Artificial Intelligence 2018, UAI 2018*.

A Derivations

A.1 Derivation of the Training Objective

We derive the training objective $\tilde{F}(\theta, \phi, q^{1:M})$ in (4) and include a derivation of the standard reparametrized diffusion objective $\mathcal{L}_D(\theta, z_0)$ analogous to Ho et al. (2020); Sohl-Dickstein et al. (2015). For convenience, we re-state the objective for a single data point here and omit the superscript m :

$$\tilde{F}(\theta, \phi, q) := \mathbb{E}_{q(z_{0:K})} \left[\log \frac{q(z_{0:K})}{p_{\theta, \phi}(x, z_{0:K})} \right]. \quad (19)$$

Simple algebra leads to:

$$\tilde{F}(\theta, \phi, q) = \underbrace{\int \int \log \frac{q(z_{1:K}|z_0)}{p_{\theta}(z_{0:K})} q(z_{1:K}|z_0) dz_{1:K}}_{\text{Diffusion Objective } \mathcal{L}_D(\theta, z_0)} q(z_0) dz_0 - \underbrace{\int \log \frac{p_{\phi}(x|z_0)}{q(z_0)} q(z_0) dz_0}_{\text{Decoder Objective}} \quad (20)$$

where we have assumed the independence structure of the decoder $p_{\phi}(x|z_{0:K}) = p_{\phi}(x|z_0)$. The diffusion objective $\mathcal{L}_D(\theta, z_0)$ can be re-written as:

$$\mathcal{L}_D(\theta, z_0) = \int \left(-\log p_K(z_K) + \log \frac{q_1(z_1|z_0)}{p_{\theta,1}(z_0|z_1)} + \sum_{k=2}^K \log \frac{q_k(z_k|z_{k-1})}{p_{\theta,k}(z_{k-1}|z_k)} \right) q(z_{1:K}|z_0) dz_{1:K}. \quad (21)$$

We can re-write $q_k(z_k|z_{k-1})$ using Bayes' rule as:

$$q_k(z_k|z_{k-1}) = q_k(z_{k-1}|z_k, z_0) \frac{q(z_k|z_0)}{q(z_{k-1}|z_0)}.$$

Combined with the Markov assumption $q(z_{1:K}|z_0) = q(z_K|z_0) \prod_{k=2}^K q_k(z_{k-1}|z_k, z_0)$, we can rewrite (21) above as:

$$\mathcal{L}_D(\theta, z_0) = \mathbb{E}_{q(z_{1:K}|z_0)} [D_{\text{KL}}(q(z_K|z_0) \| p(z_K)) - \log p_{\theta,1}(z_0|z_1)] \quad (22)$$

$$+ \mathbb{E}_{q(z_{1:K}|z_0)} \left[\sum_{k=2}^K D_{\text{KL}}(q_k(z_{k-1}|z_k, z_0) \| p_{\theta,k}(z_{k-1}|z_k)) \right] \quad (23)$$

Gaussian Transition Kernel. For the forward process, we take:

$$q_k(z_k|z_{k-1}) = \mathcal{N}(z_k; \sqrt{1 - \beta_k} z_{k-1}, \beta_k I) \quad (24)$$

$$q_k(z_{k-1}|z_k, z_0) = \mathcal{N}(z_{k-1}; \tilde{\mu}_k(z_k, z_0), \beta_k I) \quad (25)$$

$$\tilde{\mu}_k(z_k, z_0) = \frac{\sqrt{\bar{\alpha}_{k-1}} \beta_k}{1 - \bar{\alpha}_k} z_0 + \frac{\sqrt{\bar{\alpha}_k} (1 - \bar{\alpha}_{k-1})}{1 - \bar{\alpha}_k} z_k \quad (26)$$

where $\{\beta_k\}_{k=1}^K$ is a linear noise schedule with $\beta_k = (1 - k/K)\beta_0 + (k/K)\beta_K$. Using the notation $\alpha_k := 1 - \beta_k$ and $\bar{\alpha}_k := \prod_{j=1}^k \alpha_j$, we can derive the k -step transition kernel:

$$p(z_k|z_0) = \mathcal{N}(z_k; \sqrt{\bar{\alpha}_k} z_0, (1 - \bar{\alpha}_k) I), \quad \forall k = 1, \dots, K. \quad (27)$$

For the backward process, we take:

$$p_K(z_K) = \mathcal{N}(0, I) \quad (28)$$

$$p_{\theta,k}(z_{k-1}|z_k) = \mathcal{N}(z_{k-1}; \mu_{\theta,k}(z_k), \beta_k I) \quad \forall k = 2, \dots, K \quad (29)$$

$$p_{\theta,1}(z_0|z_1) = \mathcal{N}(z_{k-1}; \mu_{\theta,k}(z_k), I) \quad (30)$$

Using the formula for the Kullback-Leibler divergence between isotropic Gaussian distributions, we obtain:

$$D_{\text{KL}}(q_k(z_{k-1}|z_k, z_0) \| p_{\theta, k}(z_{k-1}|z_k)) = \frac{1}{2} \log \left(\frac{1 - \bar{\alpha}_k}{\beta_k} \right) - \frac{d_z}{2} + \frac{d_z \beta_k + \|\tilde{\mu}_k(z_k, z_0) - \mu_{\theta, k}(z_k)\|^2}{2(1 - \bar{\alpha}_k)} \quad (31)$$

$$D_{\text{KL}}(q(z_K|z_0) \| p_{\theta}(z_K)) = -\log(1 - \bar{\alpha}_K) + \frac{d_z(1 - \bar{\alpha}_K)^2 - d_z + \bar{\alpha}_K \|z_0\|^2}{2} \quad (32)$$

$$-\log(p_{\theta}(z_0|z_1)) = \frac{d_z}{2} \log(2\pi(1 - \bar{\alpha}_1)) + \frac{\|z_0 - \mu_{\theta, 1}(z_1)\|^2}{2(1 - \bar{\alpha}_1)}. \quad (33)$$

Note that in contrast to the standard pixel-space DDPM, we have the extra term in (32) depending on the latent z_0 ; we also use a Gaussian distribution with identity variance for $p_{\theta}(z_0|z_1)$ in (33) instead of the independent discrete decoder from Ho et al. (2020).

Reparametrization. We adopt the same ϵ -prediction reparameterization as in Ho et al. (2020) to write:

$$\mu_{\theta, k}(z_k) = \tilde{\mu}_k \left(z_k, \frac{1}{\sqrt{\alpha_k}} (z_k - \sqrt{1 - \bar{\alpha}_k} \epsilon_{\theta, k}(z_k)) \right) = \frac{1}{\sqrt{\alpha_k}} \left(z_k - \frac{\beta_k}{\sqrt{1 - \bar{\alpha}_k}} \epsilon_{\theta, k}(z_k) \right),$$

which gives:

$$D_{\text{KL}}(q_k(z_{k-1}|z_k, z_0) \| p_{\theta, k}(z_{k-1}|z_k)) = \frac{1}{2} \log \left(\frac{1 - \bar{\alpha}_k}{\beta_k} \right) - \frac{d_z}{2} + \frac{d_z \beta_k + \beta_k \|\epsilon - \epsilon_{\theta, k}(z_k)\|^2}{2\alpha_k(1 - \bar{\alpha}_k)}, \quad (34)$$

where $\epsilon \sim \mathcal{N}(0, I)$ is a random vector in \mathbb{R}^{d_z} sampled independently from a standard Gaussian. Additionally, using the forward k -step transition kernel, we can write $z_k = z_k(z_0, \epsilon) = \sqrt{\bar{\alpha}_k} z_0 + \sqrt{1 - \bar{\alpha}_k} \epsilon$. Up to a constant term independent of θ , we have the loss function $\mathcal{L}_D(\theta, z_0; \epsilon) \approx \hat{\mathcal{L}}(\theta, z_0; \epsilon, k)$, where we sample $k \sim \text{Unif}(1, \dots, K)$ and $\epsilon \sim \mathcal{N}(0, I)$. We thus have the following loss:

$$\hat{\mathcal{L}}_D(\theta, z_0; \epsilon, k) := \begin{cases} \frac{1}{2} \|z_0 - \mu_{\theta, 1}(z_1(z_0, \epsilon))\|^2 + \frac{\bar{\alpha}_K \|z_0\|^2}{2} & \text{if } k = 1 \\ \frac{\beta_k}{2\alpha_k(1 - \bar{\alpha}_k)} \|\epsilon - \epsilon_{\theta, k}(z_k(z_0, \epsilon))\|^2 + \frac{\bar{\alpha}_K \|z_0\|^2}{2} & \text{if } 2 \leq k \leq K \end{cases} \quad (35)$$

In practice, we follow the approach in Ho et al. (2020) to use a simplified version of the diffusion objective:

$$\hat{\mathcal{L}}_{\text{simple}}(\theta, z_0; \epsilon) \approx \hat{\mathcal{L}}_{\text{simple}}(\theta, z_0; \epsilon, k) := \begin{cases} \frac{1}{2} \|z_0 - \mu_{\theta, 1}(z_1(z_0, \epsilon))\|^2 + \frac{\bar{\alpha}_K \|z_0\|^2}{2} & \text{if } k = 1 \\ \|\epsilon - \epsilon_{\theta, k}(z_k(z_0, \epsilon))\|^2 + \frac{\bar{\alpha}_K \|z_0\|^2}{2} & \text{if } 2 \leq k \leq K \end{cases} \quad (36)$$

More specifically, we draw a minibatch of indices $\mathcal{B} \subseteq [M]$, standard Gaussian random variables $\epsilon^{m, n} \sim \mathcal{N}(0, I)$, and $t^{m, n} \sim \text{Unif}(1, \dots, K)$ for $m \in \mathcal{B}, n \in [N]$ to approximate the loss by:

$$\hat{\mathcal{L}}_{\text{simple}}(\theta, z_0^{\mathcal{B}, 1:N}) = \frac{1}{|\mathcal{B}|N} \sum_{(m, n) \in \mathcal{B} \times [N]} \hat{\mathcal{L}}_{\text{simple}}(\theta, z_0^{m, n}; \epsilon^{m, n}, t^{m, n}). \quad (37)$$

To simplify the notation, we will denote the one-sample approximation $\hat{\mathcal{L}}_{\text{simple}}(\theta, z_0^{m, n}; \epsilon^{m, n}, t^{m, n})$ with $\hat{\mathcal{L}}_{\text{simple}}(\theta, z_0^{m, n})$ as in Section 3.3 and we use the same simplified notation in the rest of the appendix.

A.2 The Euclidean-Wasserstein Geometry on $\mathbb{R}^{d_{\theta}} \times \mathbb{R}^{d_{\phi}} \times \mathcal{P}(\mathbb{R}^{d_z})$

To obtain the gradient flow in Section 3.1, we view the product space of parameters and probability distributions $\mathbb{R}^{d_{\theta}} \times \mathbb{R}^{d_{\phi}} \times \mathcal{P}(\mathbb{R}^{d_z})$ as a Riemannian manifold. We will equip this product space with suitable tangent spaces and Riemannian metrics, which enable us to define the gradients and perform optimization. We omit the subscript on z_0 and denote it by z for simplicity throughout this section.

Tangent spaces. We first note that it is equivalent to derive the gradient flow on the combined $\mathbb{R}^D \times \mathcal{P}(\mathbb{R}^{d_z})$, where $D = d_\theta + d_\phi$ is the sum of dimensions of the parameter spaces. Using the same set-up as in [Kuntz et al. \(2023\)](#), we denote the parameter space as $\Theta = \mathbb{R}^D$, and we assume the approximate posterior is a distribution with strictly positive densities w.r.t. the Lebesgue measure and have support $Z = \mathbb{R}^{d_z}$. We let the product manifold be $M := \Theta \times \mathcal{P}(Z)$. For each point $(\theta, q) \in M$, we can define the tangent space TM and its dual T^*M as:

$$\begin{aligned} T_{(\theta, q)}M &= T_\theta\Theta \times T_q\mathcal{P}(Z) \\ T_{(\theta, q)}^*M &= T_\theta^*\Theta \times T_q^*\mathcal{P}(Z) \end{aligned}$$

where we note that $T_\theta\Theta \cong T_\theta^*\Theta \cong \mathbb{R}^D$. We also define the tangent and cotangent space of $\mathcal{P}(Z)$ at q as in [Otto \(2001\)](#); [Ambrosio et al. \(2021\)](#):

$$\begin{aligned} T_q\mathcal{P}(Z) &:= \left\{ m : Z \rightarrow \mathbb{R} : \int m(z)dz = 0 \right\} \\ T_q^*\mathcal{P}(Z) &:= \{f : Z \rightarrow \mathbb{R}\} / \mathbb{R} \end{aligned}$$

where the cotangent space $T_q^*\mathcal{P}(Z)$ is identified with the space of equivalence classes of functions that differ by an additive constant.

Furthermore, we define the *duality pairing*, which is a triplet $(T_q\mathcal{P}(Z), T_q^*\mathcal{P}(Z), \langle \cdot, \cdot \rangle)$ with $\langle \cdot, \cdot \rangle : T_q\mathcal{P}(Z) \times T_q^*\mathcal{P}(Z) \rightarrow \mathbb{R}$ given by:

$$\langle m, f \rangle := \int f(z)m(z)dz, \quad \forall m \in T_q\mathcal{P}(Z), f \in T_q^*\mathcal{P}(Z). \quad (38)$$

Henceforth, we omit the local dependence of tangent space TM on (θ, q) for the sake of simplicity.

The metric. We can thus equip the manifold M with Riemannian metric $g = (g_{(\theta, q)})_{(\theta, q) \in M}$ defined as:

$$g_{(\theta, q)}((\tau, m), (\tau', m')) := \langle (\tau, m), G_{(\theta, q)}(\tau', m') \rangle \quad \forall (\theta, q) \in M.$$

where $G_{(\theta, q)} : TM \rightarrow T^*M$ is an invertible, self-adjoint, and positive-definite linear map. We will only consider tensors in a 'block-diagonal' form (cf. [Lee \(2018, Chapter 2\)](#)), which defines the metric via:

$$\langle (\tau, m), G_{(\theta, q)}(\tau', m') \rangle = \langle \tau, G_\theta\tau' \rangle + \langle m, \mathbf{G}_q^W m' \rangle \quad \forall (\tau, m) \in TM, (\theta, q) \in M. \quad (39)$$

Here we take $G_\theta : T\Theta \rightarrow T^*\Theta$ as the identity map (which corresponds to the usual Euclidean metric) and $\mathbf{G}_q^W : T\mathcal{P}(Z) \rightarrow T^*\mathcal{P}(Z)$ to be the tensor for Wasserstein-2 distance on $\mathcal{P}(Z)$ defined through its inverse:

$$(\mathbf{G}_q^W)^{-1}f := -\nabla_z \cdot (q\nabla_z f), \quad \forall f \in C^\infty(\mathcal{P}(Z)). \quad (40)$$

The gradient. To perform gradient descent on manifolds, we further need an analogue of the gradient for a smooth function $F : M \rightarrow \mathbb{R}$ as in the Euclidean space. This is a vector field $\nabla F : M \rightarrow TM$ satisfying:

$$g_{(\theta, q)}(\nabla F(\theta, q), (\tau, m)) = \lim_{t \rightarrow 0} \frac{F(\theta + t\tau, q + tm) - F(\theta, q)}{t} \quad \forall (\tau, m) \in TM, (\theta, q) \in M. \quad (41)$$

By expressing in local coordinates, we can compute the gradient as:

$$\nabla F(\theta, q) = G_{(\theta, q)}^{-1} \delta F(\theta, q), \quad \forall (\theta, q) \in M, \quad (42)$$

where $\delta F : M \rightarrow T^*M$ is the first variation of F defined as the unique cotangent vector field satisfying:

$$\langle (\tau, m), \delta F(\theta, q) \rangle = \lim_{t \rightarrow 0} \frac{F(\theta + t\tau, q + tm) - F(\theta, q)}{t} \quad \forall (\tau, m) \in TM, (\theta, q) \in M. \quad (43)$$

A.3 Derivation of the Gradient Flow

Equipped with the tools above, we now give a derivation of the gradients with respect to the distribution q for the free energy functional $\tilde{F}(\theta, \phi, q)$ in (19). We first need to compute the first variation (43) of the functional:

Lemma A.1. *Given the free energy of the form in (20):*

$$\tilde{F}(\theta, \phi, q) = \int \mathcal{L}_D(\theta, z)q(z)dz - \int \log \left(\frac{p_\phi(x|z)}{q(z)} \right) q(z)dz. \quad (44)$$

The first variation $\delta\tilde{F}(\theta, \phi, q) = (\delta_q\tilde{F}(\theta, \phi, q), \delta_\theta\tilde{F}(\theta, \phi, q), \delta_\phi\tilde{F}(\theta, \phi, q))$ is given by:

$$\delta_q\tilde{F}(\theta, \phi, q) = \log \left(\frac{q(z)}{p_\phi(x|z)} \right) + \mathcal{L}_D(\theta, z) \quad (45)$$

$$\delta_\theta\tilde{F}(\theta, \phi, q) = \int \nabla_\theta \mathcal{L}_D(\theta, z)q(z)dz \quad (46)$$

$$\delta_\phi\tilde{F}(\theta, \phi, q) = - \int \nabla_\phi \log p_\phi(x|z)q(z)dz \quad (47)$$

Proof. For eqs. (46) and (47), it suffices to note that by grouping the parameters into $\tilde{\theta} := (\theta, \phi) \in \Theta = \mathbb{R}^D$, we can compute by Taylor expansion:

$$\begin{aligned} \tilde{F}(q, \tilde{\theta} + t\tau) &= \tilde{F}(q, \tilde{\theta}) + \int f(\tilde{\theta}, z)q(z)dz - \int f(\tilde{\theta} + t\tau, z)q(z)dz \\ &= \tilde{F}(q, \tilde{\theta}) - \int [t\langle \tau, \nabla_{\tilde{\theta}} f(\tilde{\theta}, z) \rangle + o(t)]q(z)dz \\ &= \tilde{F}(q, \tilde{\theta}) - t \left\langle \tau, \int \nabla_{\tilde{\theta}} f(\tilde{\theta}, z)q(z)dz \right\rangle + o(t) \end{aligned}$$

where we have set $f(\tilde{\theta}, z) := \mathcal{L}_D(\theta, z) - \log p_\phi(x|z)$ and used $f(\tilde{\theta} + t\tau, z) = f(\tilde{\theta}, z) + t\langle \tau, \nabla_{\tilde{\theta}} f(\tilde{\theta}, z) \rangle + o(t)$.

For (45), we recall the first variation is linear, thus it suffices to compute $\delta_q \int \mathcal{L}_D(\theta, z)q(z)dz$ and $\delta_q \int \log \left(\frac{q(z)}{p_\phi(x|z)} \right) q(z)dz$ separately. Now note that:

$$\int \mathcal{L}_D(\theta, z)[q(z) + tm(z)]dz = \int \mathcal{L}_D(\theta, z)q(z)dz + t \int \mathcal{L}_D(\theta, z)m(z)dz$$

and for the latter we note that $\log(z+t)(z+t) = \log(z)z + [\log(z) + 1]t + o(t)$, from which it follows:

$$\begin{aligned} \int \log \left(\frac{q(z) + tm(z)}{p_\phi(x|z)} \right) [q(z) + tm(z)]dz &= \int (\log q(z))q(z) + [\log q(z) + 1]tm(z) + o(t)dz \\ &\quad - \int \log p_\phi(x|z)q(z)dz - t \int \log p_\phi(x|z)m(z)dz \\ &= \int \log \left(\frac{q(z)}{p_\phi(x|z)} \right) q(z)dz \\ &\quad + t \int \log \left(\frac{q(z)}{p_\phi(x|z)} \right) m(z)dz + o(t) \end{aligned}$$

where we have used that $\int m(z)dz = 0$ for all $m \in \mathcal{TP}(\mathcal{Z})$. □

Proposition A.2. *Under the product of Wasserstein-2 and Euclidean metric as in Appendix A.2,*

the gradients of the free energy $\tilde{F}(\theta, \phi, q)$ with respect to (θ, ϕ, q) are given by:

$$\nabla_{\theta} \tilde{F}(\theta, \phi, q) = \int [\nabla_{\theta} \mathcal{L}_D(\theta, z)] q(z) dz \quad (48)$$

$$\nabla_{\phi} \tilde{F}(\theta, \phi, q) = - \int [\nabla_{\phi} \log p_{\phi}(x|z)] q(z) dz \quad (49)$$

$$\nabla_q \tilde{F}(\theta, \phi, q) = \nabla_z \cdot \left[q(z) \nabla_z \left[\log \left(\frac{p_{\phi}(x|z)}{q(z)} \right) - \mathcal{L}_D(\theta, z) \right] \right] \quad (50)$$

Proof. Recall that on the manifold $M = \Theta \times \mathcal{P}(\mathbf{Z})$, the gradient can be computed from the first variation via the metric tensor (42):

$$\nabla_{(\tilde{\theta}, q)} \tilde{F}(\tilde{\theta}, q) = G_{(\tilde{\theta}, q)}^{-1} \delta \tilde{F}(\tilde{\theta}, q) = ((G_{\theta})^{-1} \delta_{\theta} \tilde{F}(\tilde{\theta}, q), (\mathbf{G}_q^W)^{-1} \delta_q \tilde{F}(\tilde{\theta}, q)),$$

where $\tilde{\theta} = (\theta, \phi)$. For the parameters θ, ϕ , their gradients are given by the usual Euclidean gradients. For the distribution q , we recall the Wasserstein-2 metric tensor $(\mathbf{G}_q^W)^{-1} f = -\nabla_z \cdot (q \nabla_z f)$ for all $f \in C^{\infty}(\mathcal{P}(\mathbf{Z}))$, which gives the desired result using Lemma A.1. \square

A.4 The Full Training Algorithm

We detail the algorithmic considerations in Section 3.3 and provide the pseudocode for practical training in Algorithm 2.

A.4.1 KL Divergence Annealing

We note that annealing the KL divergence with γ_t is equivalent to applying the same weighting to the gradient of the entropy and the prior terms. In our case, we modify the gradient flow in (8–11) as follows:

$$\nabla_{\theta} \tilde{F}(\theta_t, \phi_t, q_t^{1:M}) = \frac{1}{M} \sum_{m=1}^M \mathbb{E}_{q_t^m(z_{0,t})} [\nabla_{\theta} \gamma_t \mathcal{L}_D(\theta_t, z_0)], \quad (51)$$

$$\nabla_{\phi} \tilde{F}(\theta_t, \phi_t, q_t^{1:M}) = -\frac{1}{M} \sum_{m=1}^M \mathbb{E}_{q_t^m(z_{0,t})} [\nabla_{\phi} \log p_{\phi_t}(x^m|z_{0,t})], \quad (52)$$

$$\nabla_{q^m} \tilde{F}(\theta_t, \phi_t, q_t^{1:M}) = \nabla_{z_0} \cdot [q^m(z_{0,t}) \nabla_{z_0} \log p_{\phi_t}(x^m|z_{0,t})] \quad (53)$$

$$- \gamma_t \nabla_{z_0} \cdot [q^m(z_{0,t}) \nabla_{z_0} [\log q^m(z_{0,t}) - \mathcal{L}_D(\theta_t, z_{0,t})]], \quad \forall m \in [M] \quad (54)$$

which correspond to the Fokker-Planck equation of the following system of SDEs:

$$d\theta_t = -\frac{1}{M} \sum_{m=1}^M \mathbb{E}_{q_t^m(z_0)} [\nabla_{\theta} \gamma_t \mathcal{L}_D(\theta_t, Z_{0,t}^m)] dt, \quad (55)$$

$$d\phi_t = \frac{1}{M} \sum_{m=1}^M \mathbb{E}_{q_t^m(z_0)} [\nabla_{\phi} \log p_{\phi_t}(x^m|Z_{0,t}^m)] dt, \quad (56)$$

$$dZ_{0,t}^m = \nabla_{z_0} [\log(p_{\phi_t}(x^m|Z_{0,t}^m)) - \gamma_t \mathcal{L}_D(\theta_t, Z_{0,t}^m)] dt + \sqrt{2\gamma_t} dW_t^m, \quad \forall m \in [M] \quad (57)$$

Thus, we only need to adjust the amount of noise injected to the in (17) by setting $\sqrt{2h_z}$ to $\sqrt{2h_z \gamma_t}$ and weigh the diffusion loss $\mathcal{L}_D(\theta, z_0)$ by γ_t . Using the KL annealing scheme and re-weighted diffusion loss (36) discussed in Section 3.3, we thus modify the loss in (18) with:

$$\hat{\mathcal{L}}(\theta_t, \phi_t, z_{0,t}^{1:M, 1:N}) := \frac{1}{N|\mathcal{B}|} \sum_{(m,n) \in \mathcal{B} \times [N]} \left[\gamma_t \hat{\mathcal{L}}_{\text{simple}}(\theta_t, z_{0,t}^{m,n}) - \log p_{\phi}(x_m|z_{0,t}^{m,n}) \right], \quad (58)$$

where $\hat{\mathcal{L}}_{\text{simple}}$ is the simplified diffusion loss in Appendix A.1 and we take $\gamma_t = c_{KL} \min(1, t/T)$ for T the number of KL warm-up steps and c_{KL} a constant coefficient.

A.4.2 Preconditioning and Momentum

To avoid flat minima and ill-conditioning, we use an adaptive version of Langevin dynamics similar to Li et al. (2016); Kim et al. (2020) based on Adam (Kingma and Ba, 2014). In particular, we update each particle by running:

$$z_{0,t+1}^{m,n} \leftarrow z_{0,t}^{m,n} + Nh_z G_t^{m,n} M_t^{m,n} + \sqrt{\frac{2h_z}{M}} (G_t^{m,n})^{1/2} W_t^{m,n}, \quad \forall (m,n) \in [M] \times [N] \quad (59)$$

where h_z is the stepsize of particle updates, and we compute the moment $M_t^{m,n}$ and the preconditioner $G_t^{m,n}$ by:

$$M_t^{m,n} \leftarrow aM_{t-1}^{m,n} + N(1-a)\nabla_{z_0^{m,n}} \hat{\mathcal{L}}(\theta_t, \phi_t, z_{0,t}^{1:M,1:N}) \quad (60a)$$

$$V_t^{m,n} \leftarrow bV_{t-1}^{m,n} + (1-b)\text{diag} \left(\left[N\nabla_{z_0^{m,n}} \hat{\mathcal{L}}(\theta_t, \phi_t, z_{0,t}^{1:M,1:N}) \right]^{\otimes 2} \right) \quad (60b)$$

$$G_t^{m,n} \leftarrow (V_t^{m,n} + \epsilon I)^{-1/2} \quad (60c)$$

Here $\hat{\mathcal{L}}$ is defined as in (58), $\epsilon > 0$ is a positive constant to avoid numerical instabilities, $0 < a, b < 1$ are hyperparameters like in Adam (Kingma and Ba, 2014) (we take $a = 0.9, b = 0.999$ following the default), and we used the notation $\text{diag}(v^{\otimes 2})$ to denote the diagonal matrix with the $(i, j)^{th}$ entry being $v_i^2 \delta_{ij}$. In practice, we set the preconditioner on the noise in (59) to $G_t^{m,n} = I$ during the first epoch for numerical stability.

We now present the full algorithm for training:

Algorithm 2 IPLD with adaptive Langevin dynamics

- 1: **Inputs:** Training data points $\{x_m\}_{m \in [M]}$, optimizers $\text{Opt}_\theta, \text{Opt}_\phi$, Step sizes h_θ, h_ϕ, h_z , KL weights γ_t , Initial particles $\{z_{0,0}^{m,n}\}_{(m,n) \in [M] \times [N]}$ sampled from $\mathcal{N}(0, I)$, Initial parameters ϕ, θ .
 - 2: **while** not converged **do**
 - 3: Sample a mini-batch of indices $\mathcal{B} \subset [M]$
 - 4: Compute the loss $\hat{\mathcal{L}}(\theta_t, \phi_t, z_{0,t}^{1:M,1:N})$ as in (58)
 - 5: **for** $(m, n) \in \mathcal{B} \times [M]$ **do** ▷ Update the particle cloud
 - 6: Compute momentum $M_t^{m,n}$ and preconditioner $G_t^{m,n}$ as in (60)
 - 7: $z_{0,t+1}^{m,n} \leftarrow z_{0,t}^{m,n} + Nh_z G_t^{m,n} M_t^{m,n} + \sqrt{\frac{2h_z \gamma_t}{M}} (G_t^{m,n})^{1/2} W_t^{m,n}$
 - 8: **end for** ▷ Update model parameters
 - 9: $\theta_{t+1} \leftarrow \text{Opt}_\theta(h_\theta, \theta_t, \hat{\mathcal{L}})$
 - 10: $\phi_{t+1} \leftarrow \text{Opt}_\phi(h_\phi, \phi_t, \hat{\mathcal{L}})$
 - 11: **end while**
 - 12: **return** $\theta_t, \phi_t, z_{0,t}^{1:M,1:N}$
-

B Experimental Details

For simplicity, we use a Gaussian decoder with identity covariance $p_\phi(x|z_0) = \mathcal{N}(x; g_\phi(z_0), I)$ throughout the experiments, where g_ϕ is the decoder network parametrized by ϕ . We also fix the noise schedule $\{\beta_k\}_{k=1}^K$ as the linear schedule used in Ho et al. (2020) with $\beta_0 = 1 \times 10^{-4}$ and $\beta_K = 0.02$ with $K = 1000$.

B.1 Details on the synthetic experiments

Data. We create the training data by first drawing 10,000 samples from: 1) a GMM with 25 components of dimension $d_z = 2$ as in Boys et al. (2024); Cardoso et al. (2024), and 2) a concentric circle distribution also of dimension $d_z = 2$ similar to that in scikit-learn²(Buitinck et al.,

²https://scikit-learn.org/stable/modules/generated/sklearn.datasets.make_circles.html

2013), then we project the data into a higher-dimensional ambient space with dimension $d_x = 64$ using matrices $A \in \mathbb{R}^{d_z \times d_x}$ with orthogonal rows. We generate the matrices using the default implementation in PyTorch of orthogonal weight initialization (Saxe et al., 2014). For better visualization, we set the first 2×2 block to the identity for the concentric circle dataset.

Architecture. For the diffusion backbones, we use a multi-layer perceptron (MLP) with 3 hidden layers, each having 128 hidden units and ReLU activation. The decoder is parametrized by a single linear layer which is equivalent to a matrix with dimension $d_z \times d_x$. For the DIFFUSIONVAE, we implement the encoder also using a single linear layer equivalent to a matrix of size $d_x \times 2d_z$, where it outputs the mean and diagonal of the log-covariance matrix.

Training. We train all models for 50 epochs with a batch size of 500. We use the AdamW optimizer (Loshchilov and Hutter, 2019) with a learning rate of 1×10^{-3} for all models. For IPLD, we use a version of adaptive Langevin dynamics (Kim et al., 2020) (cf. Algorithm 2) to optimize the particles; we set the step size to 1×10^{-1} for faster convergence. The KL annealing constant c_{KL} is set to 0.01 and number of warm up steps is set to 1000 (cf. Appendix A.4).

Evaluation. We report the MMD (Gretton et al., 2012) between the generated samples and the ground truth on the GMM dataset. For samples $\{x_i\}_{i=1}^m \sim P$ and $\{y_i\}_{i=1}^n \sim Q$, the unbiased Monte-Carlo estimate of MMD is defined as:

$$\text{MMD}(P, Q) \approx \frac{1}{m(m-1)} \sum_{i=1}^m \sum_{\substack{j=1 \\ j \neq i}}^m k(x_i, x_j) + \frac{1}{n(n-1)} \sum_{i=1}^n \sum_{\substack{j=1 \\ j \neq i}}^n k(y_i, y_j) - \frac{2}{mn} \sum_{i=1}^m \sum_{j=1}^n k(x_i, y_j),$$

where we use the Radial Basis Function (RBF) kernel $k : \mathbb{R}^{d_x} \times \mathbb{R}^{d_x} \rightarrow \mathbb{R}_{\geq 0}$ with a bandwidth $\gamma = 0.1$ defined as $k(x, y) = \exp(-\gamma \|x - y\|^2)$. A total of $m = n = 10,000$ samples were generated via the reverse process to compute the approximation of the MMD. We repeat the training runs with 50 different random seeds (thus different initializations) and report the mean and standard error. The error bars shown in Figure 1 are the 1-standard error $\hat{\sigma}/\sqrt{50}$, where the standard deviation $\hat{\sigma}$ is estimated using numpy’s default implementation.

B.2 Details on the image experiments

Architecture for IPLD. We adopt the Diffusion Transformer architecture DiT-S, the smallest configuration from Peebles and Xie (2023), as the backbone for our latent diffusion model. We use a patch size of 1×1 , as our latent space of dimension $4 \times 8 \times 8$ is relatively small. For the Gaussian decoder $p_\phi(x|z_0)$, we use a simplified version of VAE’s decoder without attention from Rombach et al. (2022). We comment that in line with recent discussions on latent diffusions (Dieleman, 2025), the spatial structure of the latent space is crucial for the successful training of a latent diffusion model. Therefore, we choose to use a decoder that can induce explicit spatial structures in the latents z instead of the ones used in the EBM literature (Yu et al., 2023), which compress the images to a flattened vector. However, we note our decoders have similar or smaller number of parameters than the implementation of Yu et al. (2023) (around 18 million parameters).

Architecture for DIFFUSIONVAE. We use the exact same diffusion backbone and decoder for our re-implementation of VAE with diffusion prior (Wehenkel and Louppe, 2021). For the encoder $q_\phi(z_0|x)$ of the VAE, we parametrize it with a Gaussian $\mathcal{N}(z_0; \mu_\phi(x), \Sigma_\phi)$, where Σ_ϕ is a diagonal matrix. The encoder’s architecture also follows from Rombach et al. (2022), which an inverted version of the decoder.

Training and Evaluation. As in the synthetic experiments, we use the AdamW optimizer (Loshchilov and Hutter, 2019) for with a learning rate of 2×10^{-4} for decoders (and encoder for DIFFUSIONVAE) and 1×10^{-4} for diffusion backbones; an exponential learning rate schedule with rate

	SVHN	CIFAR-10	CelebA64
z-shape	8 x 8 x 4	8 x 8 x 4	8 x 8 x 4
Base channels	128	128	128
Number residual blocks per resolution	2	2	2
Channel Multiplier	1,2,3	1,2,3	1,2,2,3
Batch Size	128	128	16
Number of Epochs	400	400	200
Diffusion Learning Rate	1e-4	1e-4	1e-4
Decoder Learning Rate	2e-4	2e-4	2e-4
Particle Step Size	5e-2	5e-2	5e-2
KL Warm-up Steps	40000	40000	40000
KL Constant Coefficient	0.001	0.01	0.01
EMA Decay Rate	0.999	0.999	0.9999
EMA Start Step	40000	40000	40000

Table 2: An overview of IPLD’s settings for the experiments. Here z-shape refers to the shape of the latent vector, which in the case of IPLD, is the shape of a single particle. We refer the readers to LDM (Rombach et al., 2022) and the implementation thereof for more details on the architecture.

$\gamma = 0.999$ was used for the decoder. For IPLD, we use adaptive Langevin dynamics (Kim et al., 2020) with step size 5×10^{-2} and exponential learning rate decay with $\gamma = 0.995$ across all configurations. Similar to Song and Ermon (2020), we maintain an Exponential Moving Average (EMA) of the weights of the diffusion model for evaluation; the hyperparameters for EMA are reported in Table 2. To evaluate the generative performance, we calculate the FID (Heusel et al., 2017) between the true data and 50,000 generated samples using the DDIM sampler (Song et al., 2021a) with 100 network function evaluations (NFEs).

B.3 Warming-up with one particle

For the image experiments, we use a warm-started approach (Kuntz et al., 2023) for faster training. Namely, we initiate IPLD with a single particle $\{z_m\}_{m \in [M]}$ and run Algorithm 2 for 200 epochs on SVHN and CIFAR-10 (100 on CelebA64) before switching to $N > 1$ particles by replicating the each particle $\{z_m\}_{m \in [M]}$ for N times. We point out that due to the noise added in Langevin dynamics, the particles do not collapse to a single point.

B.4 Computational Resources

For all experiments, we use NVIDIA GPUs. We use a single RTX 3090 for all synthetic experiments. For image experiments, the 10-particle version of IPLD training runs on CIFAR-10 and SVHN datasets were performed on two RTX A6000 GPUs or a single A100 GPU. The remaining image experiments were performed on a single L40S GPU. Our longest experiment takes about 27 hours on a single A100 GPU, which is around 2.5 GPU days measured in V100 using the conversion rule in Rombach et al. (2022).

C Additional Numerical Results

C.1 Interpolating the Latent Space

As a deep LVM, IPLD is able to learn a smooth latent space, enabling semantically meaningful interpolations. In Figure 4, we take two indices $m_1, m_2 \in [M]$ from the training set indices and extract the particles $z_0^{m_1,0}, z_0^{m_2,0}$ from the particle cloud. We compute the linear interpolation via $\text{lerp}(x, y, s) = sx + (1 - s)y$ between those particles for $s \in [0, 1]$ and decode back into the image space with the decoder g_ϕ .



Figure 4: Linear interpolation between the particles learned on the CelebA64 training set.

C.2 Evolution of the Particle Cloud

We also visualize how the particle cloud $z_0^{1:M, 1:N}$ evolves through the gradient flow. To achieve this, we save the particle cloud at training epochs $\{0, 5, 10, 15, 20, 25, 30, 50, 75, 90\}$ and pass them through the decoder g_ϕ (Figures 5a and 5b). We note that there is an intriguing perceptual similarity between the particle evolution and the posterior mean $\mathbb{E}[x_0|x_t]$ of a diffusion model. For comparison, we show the evolution of the posterior mean predicted in Figures 6a and 6b. The posterior mean is computed by a pretrained score network taken from Song et al. (2021a) in the pixel space via Tweedie’s formula (Efron, 2011): $\mathbb{E}[x_0|x_t] \approx (\sqrt{\bar{\alpha}_t})^{-1}[x_t + \sigma_t^2 \nabla_{x_t} \mathbf{s}_\theta(x_t, t)]$, where σ_t^2 is the variance of the reverse process and $\mathbf{s}_\theta(x_t, t)$ is the score estimating network. We remark that there have been several recent works attempting to delineate the connection between diffusion and gradient flow (Yi et al., 2023; Huang and Zhang, 2023; Franceschi et al., 2023). Our method can be thought as an attempt of learning the gradient flow via a diffusion model.

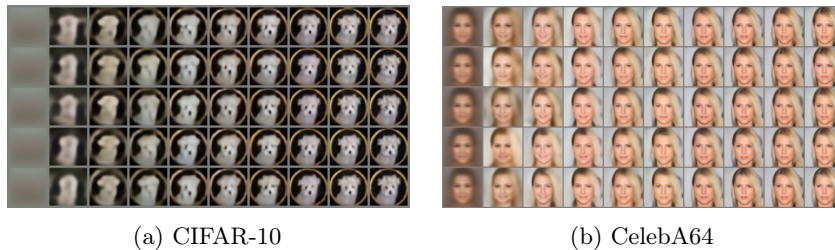


Figure 5: Evolution of the particle cloud of IPLD trained on the CIFAR-10 and CelebA64 dataset with 5 particles. Zoom in to view the details better.

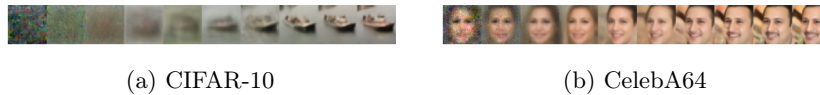


Figure 6: Evolution of the predicted $\mathbb{E}[x_0|x_t]$ of DDPM trained on the CIFAR-10 and CelebA64 dataset.

C.3 Additional Uncurated Samples

We present additional uncurated samples of IPLD trained with 10 particles on CIFAR-10, SVHN, and CelebA64 dataset produced by the DDIM sampler (Song et al., 2021a) with 100 NFEs. We remark that only the CelebA64 samples in the main text have been curated for better visualization.

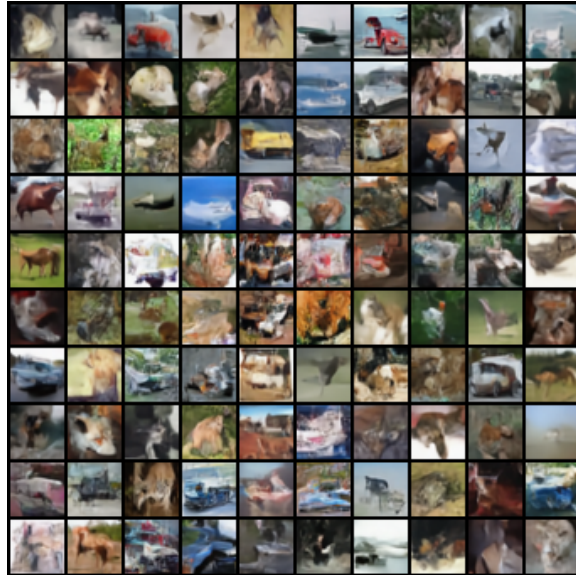


Figure 7: Uncurated samples on CIFAR-10.

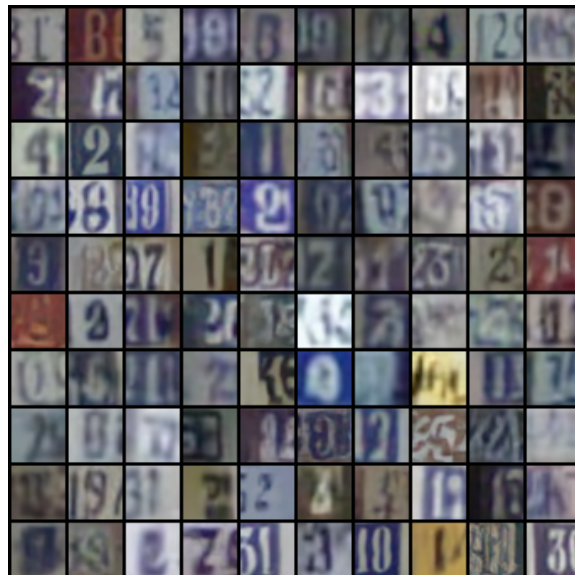


Figure 8: Uncurated samples on SVHN.

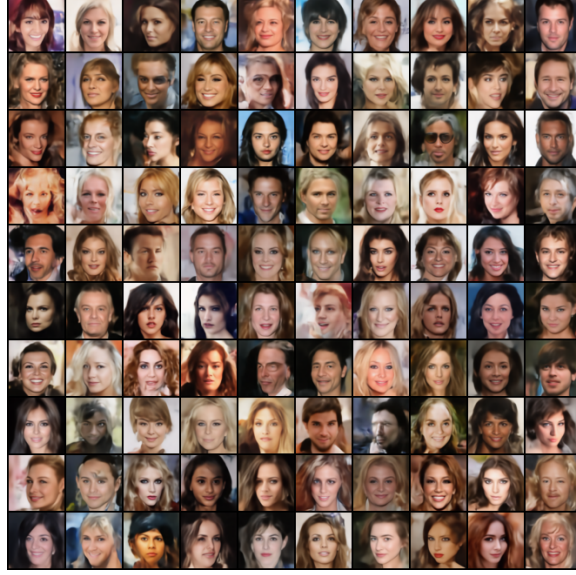


Figure 9: Uncurated samples on CelebA64.

D Proofs of Theoretical Results

Suppose that Theorem 3.1’s premise holds, and let $\lambda/2 > 0$ denote the minimum of \mathcal{R} ’s strong convexity constant and $(\theta, \phi, x, z_0) \mapsto \log(p_{\theta, \phi}(x, z_0))$ ’s strong concavity constant:

$$\nabla_{(\theta, z_0)}^2 \mathcal{R}(\theta, z_0) \succeq \lambda I, \quad \nabla_{(\theta, \phi, z_0, \phi)}^2 \log(p_{\theta, \phi}(x, z_0)) \preceq -\lambda I.$$

Given (6), it follows that, for each m in $[M]$, $(\theta, \phi, z_0) \mapsto \log(p_{\theta, \phi}(x_m, z_0))$ is λ -strongly concave. Consequently, so is

$$\ell(\theta, \phi, z_0^{1:M}) := \log \left(\prod_{m=1}^M \tilde{p}_{\theta, \phi}(x_m, z_0^m)^{1/M} \right) = \frac{1}{M} \sum_{m=1}^M \log \tilde{p}_{\theta, \phi}(x^m, z_0^m).$$

For this reason, replacing (θ, x) in (Kuntz et al., 2023, Theorem 4 in Appendix B.3) by $((\theta, \phi), z_0^{1:M})$ here tells us that $\tilde{\ell}$ has a unique maximizer. Similarly, (Caprio et al., 2024, Theorem 5) tells us that $(\tilde{p}_{\theta, \phi}(dz_0^{1:M}))_{(\theta, \phi) \in \Theta \times \Phi}$ satisfies the log-Sobolev inequality in (Caprio et al., 2024, Definition 1). The rightmost inequality in Theorem 3.1’s conclusion then follows from (Caprio et al., 2024, Theorem 1), and the leftmost one from Proposition 2.1 and (Caprio et al., 2024, Theorem 2).

Given the extra Lipschitz gradients assumption, Theorem 3.2 then follows directly from (Caprio et al., 2024, Theorem 7), see therein for the precise constants.